

MemAscend: System Memory Optimization for SSD-Offloaded LLM Fine-Tuning

Yong-Cheng Liaw, Shuo-Han Chen

Abstract—Owing to the huge success of generative artificial intelligence (AI), large language models (LLMs) have emerged as a core subclass, underpinning applications such as question answering, text generation, and code completion. While fine-tuning these models on domain-specific data can yield significant performance gains, it also poses daunting computational challenges, especially for researchers and small organizations with limited hardware resources. Although SSD offloading (i.e., ZeRO-Infinity) has emerged as a viable strategy to overcome the GPU memory barrier via leveraging both system memory (i.e., CPU DRAM) and storage space (i.e., solid-state devices, SSDs), its design primarily targets model-centric performance issues. As a result, key system-level issues, including system memory fragmentation, inefficient pinned buffer allocation, peak CPU usage spikes, and file system overhead, remain unaddressed, stifling scalability and inflating costs. Such an observation motivates this paper to introduce MemAscend, a framework that systematically tackles the underexplored system memory bottlenecks in SSD-offloaded LLM training, with a focus on resource-constrained environments. By streamlining pinned-memory allocation, eradicating fragmentation, and mitigating peak overhead, MemAscend reclaims a substantial system memory budget, enabling larger models, longer context windows, and higher batch sizes without exceeding modest hardware limits. Across diverse LLM benchmarks, MemAscend reduces peak system-memory consumption by an average of 55.7% compared with standard SSD offloading techniques, lowering the hardware barrier for fine-tuning and unlocking new possibilities for cost-effective large-scale training on limited-resource machines.

Index Terms—LLM, offloading, fine-tuning, GPU, DRAM, SSD

I. INTRODUCTION

The growth of large-language-model (LLM) applications has significantly surged in recent years, propelled by steady advances in model capabilities [1]. LLMs have now powered conversational assistants, automatic summarization, multilingual translation, and countless other tasks. To adapt LLMs to a specific domain, fine-tuning on domain-specific datasets is a widely used approach [2] to customize pre-trained foundational models and address the nuances of a specific domain better. Although fine-tuning markedly boosts reliability and task performance, it also demands considerable computation and memory usage. Commercial leaders routinely train foundation models on massive GPU clusters. For example, Meta’s Llama 3 relied on 16,000 NVIDIA H100 GPUs [3]. By contrast, academic labs, individual researchers, and small enterprises must operate within tight hardware budgets, with limited GPU count and modest system-memory capacity. Finding cost-effective ways to fine-tune LLMs under such tight resource constraints, therefore, remains an open challenge.

Broadly, LLM training consumes two memory classes: (1) **static memory**, which includes model weights and optimizer

states, and (2) **residual states**, such as activations and intermediates [4]. Static memory is substantial because modern transformers contain billions of parameters, and optimizers such as Adam store both momentum and variance for each weight [5]. Activations can also dominate due to their linear growth with batch size and sequence length [6]. Several techniques have been proposed to mitigate the above memory pressure. For instance, to lower activation memory, gradient-checkpointing [7] does not store every activation during the forward pass, but instead stores only a few checkpointed activations and recomputes those missed ones during back-propagation. Works such as Liger-Kernel [8] further fuse operations (e.g., RMSNorm, SwiGLU, Cross-Entropy [9]–[11]) into single Triton [12] kernels, eliminating transient buffers and launch overhead. Mixed-precision and related quantization techniques [13] shrink activations by casting tensors to `fp16` or `bf16`; this in turn enables memory-efficient kernels such as Flash-Attention [14].

For static memory, quantization has been widely explored. For instance, 8-bit optimizers [15] and 4-bit optimizers [16] have shown promising results in reducing static memory consumption with minimal impact on convergence speed. On the other hand, Parameter-Efficient Fine-Tuning (PEFT) [17], especially Low-Rank Adaptation (LoRA) [18], significantly reduce the number of trainable parameters by focusing on low-rank matrices while keeping the pre-trained model frozen. Although methods like LoRA offer substantial computational and memory efficiency, they often require meticulous hyper-parameter tuning, such as determining the rank and selecting which weights to train, to achieve optimal performance [19], [20]. Consequently, full-parameter training remains crucial for maximizing task-specific performance, particularly in scenarios where pre-trained models have not been exposed to domain-specific or private data. In such cases, the discrepancies between the target and pre-trained domains can be substantial, necessitating full-parameter training to bridge the gap effectively.

Although full-parameter fine-tuning can achieve optimal performance in fine-tuning scenarios, the large size of pre-trained models limits the feasibility of training in resource-limited environments. Typically, fine-tuning tasks involve relatively smaller datasets, so the primary bottleneck in resource-limited scenarios is that GPU memory or system memory resources are insufficient to handle the static and residual memory requirements of these models. To address these limitations, SSD offloading has emerged as a promising solution [21]. This technique transfers static memory, such as model weights and optimizer states, from GPUs to SSDs, which generally

provide significantly larger storage capacity. For example, ZeRO-Infinity, a state-of-the-art SSD offloading system, moves static memory to NVMe SSDs. In this approach, GPU memory is reserved for intermediate values, while system memory acts as an intermediary for transferring data between GPUs and SSDs or for performing operations, such as optimizer steps, on the CPU. This strategy reduces the volume of data transfer across the PCIe bus. Although SSD offloading may reduce training performance due to additional PCIe transfer latency, this impact is mitigated for fine-tuning tasks, which typically involve relatively smaller dataset compared to pre-trained task. Furthermore, SSD offloading integrates effectively with other optimization techniques such as Flash-Attention, Liger-Kernel, gradient checkpointing, and even advanced strategies to offload checkpointed values into system memory. By integrating these techniques, GPU memory usage is minimized, enabling the largest trainable context length or batch size, and potentially mitigating the original performance loss caused by additional data transfers across heterogeneous devices.

However, SSD offloading systems like ZeRO-Infinity are primarily designed to scale trainable model sizes on high-performance machines rather than hardware with limited system memory. While GPU memory usage has been extensively studied, system memory usage has received comparatively less attention. Several studies have explored SSD offloading techniques. For example, LoHan [22] enables fine-tuning of very large models on a single consumer-grade GPU with limited main memory through holistic tensor movement management. Although impressive in extreme resource constraints, its optimizations are specifically tailored for this single-GPU scenario and address a problem context that is different from that of enhancing the general distributed ZeRO-Infinity system. Other approaches, such as Smart Infinity [23], focus on specialized architectures that enable the computation on SSDs and are not broadly applicable to commodity hardware. In our study, we analyze the system memory requirements for SSD offloading and identify key challenges. System memory, acting as an intermediary, includes various types of pinned buffers [24] that facilitate data transfer between GPU and CPU. Inefficient management of these buffers leads to fragmentation and wasted memory. Additionally, significant peak memory overhead arises from inefficient operations involving the CPU and system memory. Furthermore, system memory may also accommodate activation checkpointed values when the offloaded activation checkpointing technique is employed. This technique stores only a few checkpointed activations and recomputes others when needed. By offloading these checkpointed values into system memory, it is possible to save substantial GPU memory space, thereby enabling the training of tasks with the largest context lengths. However, the original SSD offloading system introduces unnecessary memory overhead, which undermines the feasibility of the offloaded activation checkpointing method.

In this paper, we focus on two key types of system memory inefficiencies: fragmentation and reduction of peak memory overhead in SSD offloading scenarios. These inefficiencies arise primarily due to the limitations of existing SSD offloading systems for resource-limited machines, particularly the

constrained resources of both GPU memory and system memory. Furthermore, standard memory management practices, such as aggressive alignment in pinned memory allocation, while beneficial in other contexts, introduce significant overhead and waste in the large, static allocation patterns typical of SSD offloading. These constraints result in considerable resource wastage and hinder the potential for cost-effective SSD offloading. To address these challenges, we propose solutions that minimize system memory requirements while maximizing the trainable model size and the trainable context length within the same configuration. The contributions of this study are summarized as follows:

- 1) The issue of buffer fragmentation was addressed, with a proposed solution achieving an average reduction of 72.71% in various models.
- 2) Pinned memory allocation overhead was significantly reduced by eliminating unnecessary alignment, saving substantial system memory.
- 3) Overhead and double-up peak memory problems during overflow checks were mitigated, eliminating the 1.25x memory overhead.
- 4) Inefficiencies in the system memory to SSD I/O pathway were resolved, with a proposed solution reducing I/O latency, particularly for write operations.
- 5) Integration of a pure half-precision optimizer into the SSD offloading system reducing I/O transfer volume by 58%, improving throughput by an average of 17-27%.

In summary, while fine-tuning LLMs is essential in many cases, most machines struggle to meet the requirements for training these models. Even during the fine-tuning phase, where the dataset is relatively small compared to the trillions of tokens used in the pre-training phase, a significant number of GPUs to maximize training throughput is often unnecessary. The primary objective and bottleneck lies in accommodating the model size and extended context lengths, which demand substantial space to store static and residual state memory. An SSD offloading system shows promise in addressing these challenges by transferring static memory to SSDs. Additionally, integrating this system with techniques such as Liger-Kernel, offloaded activation checkpointing, and gradient accumulation can reduce activation memory usage and improve throughput. However, current SSD offloading systems do not efficiently manage system memory. This inefficiency limits the trainable model size and the available space for offloaded checkpoints, thereby constraining the maximum context length. Our work proposes several approaches to address the system memory bottleneck, enabling more cost-effective training for models with the desired size and context length.

The rest of this article is organized as follows. The background and motivation are detailed in Sections II and III. The design of the proposed system is introduced in Section IV. Section V provides analyses that address memory efficiency and explain how the proposed approach achieves the largest trainable model size and context length under identical configurations. The evaluation results are presented in Section VI. Finally, Section VII offers concluding remarks.

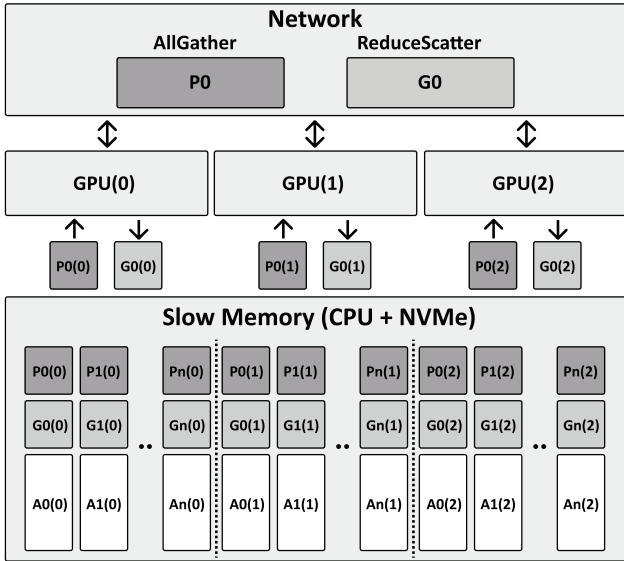


Fig. 1. ZeRO-Infinity data flow during the backward pass for an n -layer model with three data-parallel ranks. Parameters $P0(i)$ are moved to GPU, gradients $G0(i)$ are processed and offloaded, and optimizer states $A0(i)$ are updated on the CPU.

II. BACKGROUND AND RELATED WORKS

A. SSD offloading Systems

To overcome GPU memory limitations for large-scale model training, heterogeneous memory systems utilizing SSD offloading have emerged as a promising approach. These systems strategically move less frequently accessed data, primarily static model states, from expensive GPU memory to more abundant and cost-effective system memory or NVMe SSDs.

ZeRO-Infinity [21] represents a state-of-the-art SSD offloading system integrated within the DeepSpeed library [25]. It is based on the ZeRO distributed training strategy [4], [26], which partitions model states across data-parallel processes to eliminate memory redundancy. ZeRO-Infinity extends this by introducing the SSD offloading scheduler, enabling the offloading of partitioned model static states to CPU memory and subsequently to NVMe SSDs, as shown in Figure 1.

In the ZeRO-Infinity workflow, forward and backward passes are executed on the GPU, while the optimizer step is typically performed on the CPU since the compute complexity is lower than forward and backward, which is why it is not worth transferring it to the GPU for computation [26]. ZeRO-Infinity employs techniques such as bandwidth-centric partitioning and overlap-centric design to maximize data transfer efficiency across the PCIe bus and NVMe interfaces. While powerful for scaling model size, ZeRO-Infinity’s implementation, particularly its management of CPU system memory buffers for staging data between GPU and SSD, can introduce significant inefficiencies and overhead, especially on resource-limited machines with limited system memory addressed by this work.

B. Related Works in SSD offloading

1) *LoHan*: LoHan [22] focuses specifically on enabling the fine-tuning of very large models on a single consumer-grade GPU within a commodity server that has limited main

memory. It achieves this through holistic management of tensor movement, introducing techniques like active gradient offloading (overlapping CPU optimizer work with GPU backward pass) and traffic-aware activation swapping between GPU, CPU, and SSD. While LoHan demonstrates impressive capability in extreme resource constraints (e.g., fine-tuning 175B on one RTX 4090), its optimizations and design are primarily tailored for this single-GPU consumer hardware scenario. Our work, MemAscend, addresses system memory inefficiencies within the general SSD offloading system like ZeRO-Infinity, which is designed for distributed training across various scales (single node to large clusters) and does not focus solely on the single-GPU or few GPUs use case. Therefore, LoHan addresses a different problem context.

2) *SSDTrain*: SSDTrain [27] proposes an adaptive system specifically for offloading activations to NVMe SSDs to mitigate the GPU memory bottleneck caused by large activation tensors, particularly during training with large batch sizes or long sequences. Specifically, it focuses on efficiently overlapping the I/O transfers of activations with GPU computation, demonstrating significant reductions in peak activation memory usage with negligible performance overhead. SSDTrain’s approach is complementary to systems like ZeRO-Infinity (and our MemAscend), which primarily handle the offloading of static model states. Techniques for activation offloading, like SSDTrain’s, can be potentially integrated with model state offloading systems to further optimize overall memory usage. As a result, SSDTrain addresses a different component of memory and is compatible with our offloading strategy.

C. GPU Memory Efficiency Optimizations

Although SSD offloading addresses the capacity limitations for storing large model states, optimizing the usage of limited, high-bandwidth GPU memory remains crucial for performance. Several techniques enhance GPU memory efficiency and can be used in conjunction with SSD offloading systems like ZeRO-Infinity and MemAscend. By reducing the GPU memory footprint, these methods allow the system to accommodate larger models, increase batch sizes, or enable longer context lengths, potentially improving overall training throughput.

1) *Liger-Kernel*: Liger-Kernel [8] provides a library of optimized Triton kernels for common operations in LLM training, such as RMSNorm, SwiGLU, and Cross Entropy loss computation. Standard deep learning systems such as PyTorch often execute these operations using multiple separate CUDA kernel launches, leading to intermediate memory allocations and kernel launch overhead. Liger-Kernel employs kernel fusion to combine these operations into single, optimized kernels. This fusion avoids materializing large intermediate tensors (e.g., the full logit tensor before softmax in Cross Entropy), thereby reducing peak GPU memory usage and improving execution speed. By integrating Liger-Kernel, we can maximize GPU computational efficiency and minimize memory spikes during the forward and backward passes, making better use of the GPU resources freed up by SSD offloading.

2) *Flash-Attention*: Flash-Attention [14] is an I/O-aware exact attention algorithm designed to address the quadratic memory and time complexity of standard attention mechanisms, particularly for long sequences. Instead of materializing the large $N \times N$ attention matrix in GPU high-bandwidth memory, Flash-Attention uses tiling and takes advantage of faster on-chip SRAM. Calculate the output of attention block by block, significantly reducing the number of reads and writes from memory to HBM. This approach reduces the memory complexity of attention from $O(N^2)$ to $O(N)$ (linear in context length) without resorting to approximations, thus maintaining model precision. Utilizing Flash-Attention drastically cuts the GPU memory required for the attention mechanism, which is often a bottleneck for long-context training, and simultaneously speeds up computation. This works well with SSD offloading by minimizing the GPU memory required for dynamic activations.

3) *Gradient Checkpointing*: Gradient checkpointing [7], also known as activation recomputation or activation checkpointing, is a technique that trades additional compute during the backward pass for reduced GPU memory usage during the forward pass. Instead of storing all intermediate activations required for gradient calculation, only a subset of activations (checkpoints) is saved. During the backward pass, the activations needed between checkpoints are recomputed on-the-fly starting from the nearest preceding checkpoint. Various strategies exist, such as checkpointing every k layers or selectively checkpointing based on memory usage and recomputation cost. This technique significantly lowers the maximum GPU memory required for activations, making it essential for training large models or using long sequences.

4) *Offload Gradient Checkpointing*: Building upon gradient checkpointing, offload gradient checkpointing further reduces the footprint of the GPU memory by moving the saved checkpoint activations themselves from the GPU memory to the CPU system memory. During the backward pass, these checkpoints are transferred back to the GPU just before they are needed for recomputation. ZeRO-Infinity includes the capability to offload activation checkpoints to CPU memory. Unsloth [28] also provides an implementation focused on efficient CPU offloading using asynchronous transfers. While this technique dramatically frees up GPU memory, potentially enabling much longer context lengths or larger batch sizes, it makes the training process more sensitive to system memory capacity and bandwidth. Our work, MemAscend, by optimizing system memory usage and reducing overhead within the ZeRO-Infinity system, directly enhances the feasibility and effectiveness of offload gradient checkpointing. The system memory saved by MemAscend can be repurposed to store more or larger offloaded checkpoints, thus enabling larger trainable model sizes or context lengths than possible with the baseline ZeRO-Infinity under the same hardware constraints.

Although SSD offloading systems like ZeRO-Infinity provide a foundation for training massive models by leveraging heterogeneous memory, significant inefficiencies remain, particularly in system memory management. Our work focuses on the system memory bottlenecks inherent in the SSD offloading system itself, with integration with other related works like

SSDTrain, Liger-Kernel, Flash-Attention, and offload gradient Checkpointing, and optimizing various aspects of memory, thereby improving its overall efficiency and scalability across various configurations and enabling better synergy with other optimization techniques.

III. OBSERVATION AND MOTIVATION

A. System Memory Fragmentation Challenge

In an SSD offloading system, there is a system memory buffer pool fragmentation issue that occupies more system memory than necessary. This buffer is due to the fact that all model weights are stored in SSD storage and the system pre-fetches only the necessary weights during forward or backward propagation.

To facilitate this process, the system implements a buffer pool that manages all pre-allocated pinned memory. When a layer’s weights need to be fetched, the buffer pool assigns a pinned system memory buffer to it. The process involves performing I/O operations to load the weight tensor from the SSD into the pinned system memory, followed by a host-to-device copy to transfer the data to the GPU. Once the weight is no longer needed, the pinned system memory buffer is released and returned to the buffer pool. Each pinned memory buffer within the buffer pool is the same size, and the number of buffers depends on the model architecture. Since the buffer is needed every time a PyTorch submodule performs a forward operation, it is challenging to analyze statically and can dynamically change if different activation optimization algorithms are enabled (e.g., gradient checkpointing changes the frequency with which submodule within the model invokes forward operations). However, in the general case, the buffer size is designed to fit the weights of one to a few transformer blocks.

The main issue is that the buffer size is determined by the largest weight tensor, leading to internal fragmentation. Modern models typically have an embedding layer with a significantly larger weight size compared to other layers. For instance, in the Llama 3 8 billion model, the embedding layer size is determined by a vocabulary size of 128,256 multiplied by a hidden size of 5,120, whereas other layers are much smaller. For example, the second largest weights in the model are usually the up, gate, and down projection layers in the feed-forward network, with sizes of $14,336 \times$ hidden size 5,120, which are smaller than the embedding layer. The smallest swappable layer is the key and value projection, with a size of $1,024 \times$ hidden size 5,120. The disparity in the sizes of the tensors exacerbates fragmentation. As a result, the total buffer size required is 13.05 GiB, while the actual swappable tensor size needed at any given time is only 3.81 GiB, leading to a 70.82% fragmentation problem.

B. Inefficiency in Pinned Memory Allocation

Pinned (or page-locked) memory is essential for efficient data transfers in SSD offloading systems like ZeRO-Infinity. System memory acts as a staging ground between high-speed GPU memory and slower, high-capacity SSD storage. GPUs require data to reside in pinned memory before initiating

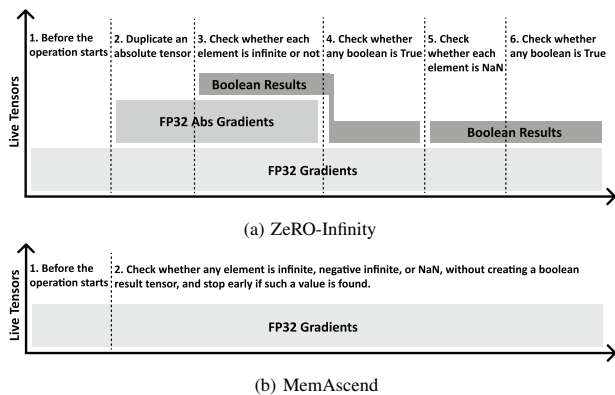


Fig. 2. Comparison of tensor lifetimes during gradient overflow checks in SSD offloading.

Direct Memory Access (DMA) over PCIe. Bypassing the extra copy from pageable memory to a pinned buffer managed by the driver significantly reduces latency and CPU load. To avoid this overhead, systems often pre-allocate pinned memory buffers for frequently transferred tensors, such as model weights fetched from SSD or gradients being offloaded. Standard memory allocators in deep learning frameworks, particularly PyTorch’s `CachingHostAllocator`, can introduce substantial inefficiencies in this context. The allocator caches pinned memory and rounds each requested size S up to the next power of two. This alignment minimizes fragmentation in workloads with frequent, variably sized allocations and deallocations, but it becomes inefficient when applied to SSD offloading.

In SSD offloading, pinned memory allocations tend to be large and long-lived. Flat buffers for gradient partitions, staging areas for optimizer states, and large tensors such as embeddings are typically allocated once and persist throughout training. When such buffers, often hundreds of MiB or several GiB, are aligned to the next power of two, the internal fragmentation becomes significant. For instance, an allocation slightly over 2 GiB may be rounded up to 4 GiB, wasting nearly 2 GiB. The original motivation for this alignment, which is avoiding fragmentation in dynamic allocation patterns, does not apply when the allocations are large and static. Reducing this alignment overhead is critical for efficient memory use in SSD offloading systems.

C. Peak Memory Bottlenecks in System Memory

In ZeRO-Infinity, the flat buffer for gradient partitioning is a contiguous memory block that holds partitioned gradients to streamline communication and computation during distributed training. With gradient accumulation enabled, this buffer supports seamless accumulation. When ZeRO-Offload or ZeRO-Infinity is active, the buffer resides in system memory, allowing efficient transfer of temporary GPU results into it.

A key limitation, however, is that the buffer size mirrors the model parameter size. To support accumulation across iterations, the buffer typically uses fp32 even when forward and backward passes run in fp16. This becomes a major bottleneck in large-scale models, as the flat buffer size grows with model complexity. As shown in Figure 2(a), the peak memory usage primarily stems from gradient overflow checks.

In mixed-precision training with fp16, overflows can occur in intermediate results, requiring a check after every iteration. If an overflow is found, the system reduces the scaling factor to prevent future instability. This check introduces two main challenges.

First, the memory overhead of detecting overflows is significant. Three conditions must be evaluated: infinity, negative infinity, and NaN. In PyTorch, this involves calling `isinf()` followed by `any()`. Internally, `isinf()` triggers `isabs()` to duplicate the tensor before performing comparisons, which creates a temporary copy and a Boolean tensor, resulting in a memory spike to about 2.25× the original size. `isnan()` avoids `isabs()` but still produces a Boolean tensor, adding another 1.25× memory peak. For example, when training an 8-billion-parameter model, the flat buffer on the CPU consumes 29.91 GiB, but the overflow check pushes usage to 67.30 GiB. Second, the sequence of operations in the overflow check introduces significant latency: (1) `isabs()`, (2) `isinf()`, (3) `any()`, (4) `isnan()`, and (5) `any()`. This chain of steps adds roughly 5507 ms per iteration for an 8-billion-parameter model on the Configuration 1 machine described in Table II, substantially slowing training. Since this check runs every iteration, the cumulative impact on performance is considerable.

D. Filesystem Overhead in SSD offloading

In the SSD offloading system, the SSD serves as extended memory. It stores low-precision compute weights, such as fp16, along with the full-precision fp32 master weights, gradients, and optimizer states. These data are loaded or offloaded depending on the computational context. The current implementation uses the filesystem with the `O-DIRECT` flag, which bypasses the page cache to ensure that data transfers go directly to the SSD. Each tensor is offloaded to a separate file, allowing the filesystem, such as ext4, to manage storage allocation without direct intervention. However, writing to ext4 carries overhead. The filesystem maintains metadata for each file, including name, size, permissions, and timestamps, which requires additional I/O and increases latency. Allocating disk blocks can also involve searching for contiguous space, updating allocation tables, and maintaining alignment, all of which add computational cost and risk fragmentation. When the SSD is used as an extension of memory and subjected to sustained I/O, these filesystem overheads accumulate. This added latency can limit the efficiency gains expected from offloading, particularly during training.

E. Motivation

The inefficiencies described above, including buffer fragmentation, overhead from pinned memory allocation, and memory spikes during tasks like gradient overflow checks, lead to substantial system memory waste. While SSD offloading already enables training significantly larger models on machines with limited resources, as shown in Table I under a 128 GiB system memory cap, it still hits a hard ceiling. Regardless of whether the setup involves a single GPU or multiple, system memory bottlenecks inherent to SSD

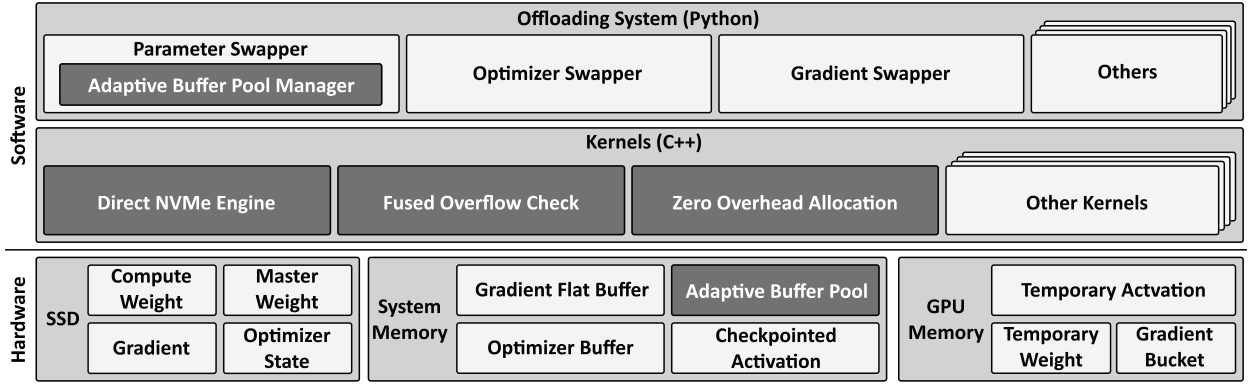


Fig. 3. System architecture of MemAscend, highlighting optimized low-level kernels and memory management for reduced memory usage and enhanced performance.

offloading limit scalability and undercut cost-efficiency. This work aims to eliminate those inefficiencies within the SSD offloading context. Reducing system memory waste brings clear advantages across all SSD offloading scenarios. It either allows training larger models within the same memory limits or reduces the hardware required for current models, improving cost efficiency. The saved memory space can also store more offloaded activation checkpoints, which supports longer context lengths or larger batch sizes. This not only extends the feasible model scale and input capacity, it also improves training throughput by increasing computation per I/O cycle. Addressing overheads like I/O latency and overflow check times further enhances efficiency and scalability.

TABLE I
PEAK SYSTEM MEMORY USAGE COMPARISON ON DIFFERENT TRAINING MODEL SIZE ACROSS DIFFERENT TRAINING SYSTEM APPROACHES.

Type	Model	Peak DRAM (GiB)
All in GPU	1B	4.48
ZeRO-Offload	1B	42.99
ZeRO-Infinity	1B	39.04
All in GPU	3B	N/A (VRAM OOM)
ZeRO-Offload	3B	104.17
ZeRO-Infinity	3B	62.97
All in GPU	8B	N/A (VRAM OOM)
ZeRO-Offload	8B	N/A (DRAM OOM)
ZeRO-Infinity	8B	91.76

IV. METHODS

A. Overview of Methods

This study presents a set of optimizations to address critical memory inefficiencies in SSD offloading systems. The approach targets four primary issues: system memory fragmentation in buffer pool management and pinned memory allocation, peak memory usage due to gradient overflow checks, and file system overhead in SSD offloading. To tackle these inefficiencies, the approach employs four key optimizations. First, an adaptive buffer pool strategy reduces internal fragmentation caused by monolithic buffer allocations. Second, a custom memory allocator minimizes waste from excessive alignment. Third, a fused kernel leverages OpenMP to perform efficient gradient overflow checks, reducing memory spikes and operation latency. Fourth, a direct SSD space management scheme replaces the filesystem-based SSD offloading mechanism, eliminating metadata overhead and lowering I/O latency.

The approach integrates into the ZeRO-Infinity framework, which combines SSD offloading, gradient checkpointing, and the Liger Kernel to enhance GPU memory efficiency. These optimizations improve performance, alleviate memory pressure, and enable larger batch sizes or longer context windows by freeing system memory for activation offloading.

Figure 3 illustrates the MemAscend architecture. The approach affects three distinct stages of the training process. During initialization, the system allocates various buffers, including gradient partition flat buffers, buffer pools for optimizer states, and other critical allocations. Instead of relying on PyTorch’s default pinned memory mechanism, MemAscend uses a Zero Overhead Allocation C++ kernel to reduce unnecessary alignment and fragmentation. In the layer-wise forward and backward passes, the system pre-fetches weight tensors from SSD to CPU, then transfers them to the GPU for an all-gather operation. A hook linked to this transfer activates the parameter swapper, which moves tensors from the SSD to system memory. The swapper queries the Adaptive Buffer Pool to secure a buffer matching the current layer’s size. Once allocated, the buffer manager invokes the Direct NVMe Engine to execute the required I/O operations. After loading, the data transfer to GPU memory, and the buffer is released. This cycle repeats across layers during training. In the final stage, before the optimizer step, the system verifies that accumulated gradients have not overflowed. A Fused Overflow Check Kernel performs a single-pass check with minimal memory overhead and computation, reducing redundancy.

B. Adaptive Buffer Pool

To mitigate system memory fragmentation, a precise understanding of buffer requirements is essential. These requirements are primarily driven by data transfer demands between SSDs and GPUs during layer-wise forward and backward propagation and commonly employ asynchronous prefetching. Due to pre-fetching operations that will cause N number of blocks concurrently in flight, the required buffer capacity is for N transformer blocks. In each transformer blocks, since smaller tensors can remain permanently in CPU memory, the primary tensors requiring transfer include the feedforward layer weights, specifically the up, down, and gate projections, and the attention layer weights, namely the Q, K, V, and O

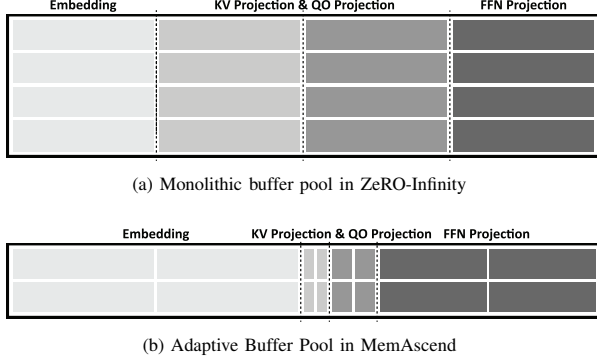


Fig. 4. Comparison of parameter buffer pool management in SSD offloading.

projections. Additionally, dedicated buffers are required for the embedding layer weights and the final linear layer weights, often referred to as the LM head. Thus, the overall buffering strategy must accommodate weights for one embedding layer, N transformer blocks each containing multiple weight tensors, and one LM head.

Compared to the original SSD offloading system, which suffers from internal fragmentation inherent in the monolithic buffer pool approach, our proposed adaptive memory buffer pool architecture addresses this limitation by implementing distinct pools for different tensor shapes. Given that embedding and LM head weights share identical dimensions (vocabulary size \times hidden size), and feedforward projections maintain consistent dimensions (intermediate size \times hidden size), we establish four specialized pools: embedding-related weights, feedforward projections, K and V projections (commonly identical in models employing grouped-query attention), and Q and O projections. These groups maintain counts of 2, $3N$, $2N$, and $2N$, respectively, effectively eliminating internal fragmentation.

This approach is effective not only for single-GPU setups, in multi-GPU configurations employing parameter partitioning, each process fetches only its assigned shard of a tensor. Consequently, the individual buffer sizes required per process are reduced proportionally to the number of partitions. However, from a system wide perspective, the aggregate buffer capacity remains consistent with single GPU configurations. Therefore, the proposed adaptive buffer pool optimization maintains its effectiveness across various distributed GPU setups.

As illustrated in Figure 4, this adaptive approach utilizes specialized subgroups for different tensor sizes. This method significantly mitigates the internal fragmentation observed in the monolithic buffer pool characteristic of original SSD offloading systems.

C. Zero Overhead Pinned Memory Allocation

As noted in Section III-B, PyTorch’s default power-of-two alignment for pinned memory allocations causes significant memory waste, especially with large static buffers used in SSD offloading. To avoid this overhead, the standard PyTorch caching allocator is bypassed for these buffers. Instead, memory is allocated directly using system calls and

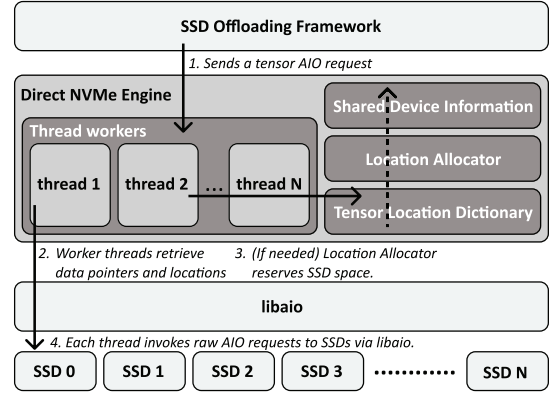


Fig. 5. Architecture and workflow of the Direct NVMe Engine for optimized SSD I/O.

CUDA runtime APIs. The required host memory is first allocated with standard memory functions, aligned only to the minimal extent required by the system. This avoids the excessive rounding imposed by power-of-two policies. The allocated region is then registered as pinned using the CUDA API `cudaHostRegister`, making it accessible for efficient GPU DMA transfers. This direct allocation and registration strategy ensures that pinned memory buffers use only the space needed for the data plus minimal alignment. It eliminates the internal fragmentation caused by power-of-two rounding and substantially reduces system memory usage for large allocations such as the gradient partition flat buffer and the adaptive buffer pool.

D. Fused Overflow Check

As mentioned in the motivation section, when the SSD offloading system checks for gradient overflows, it involves multiple operations such as `isnan()`, `isinf()`, and others. Each of these operations in PyTorch produces several intermediate values, resulting in a peak memory overhead of approximately 2.25 times the size of the flat buffer of the gradient partition, which corresponds to the model size. Performing multiple steps for a single task is inefficient. By fusing these operations into a single operation, we can reduce memory usage and improve performance.

The fused overflow check logic is illustrated in Figure 2(b). In the SSD offloading system, the flat buffer of the gradient partition is typically stored in fp32 to support gradient accumulation. While fp32 helps prevent overflow, the gradients computed during backpropagation remain in fp16, meaning overflow is still possible and must be checked in the fp32 tensors.

According to the IEEE 754 standard [29], NaN values have all exponent bits set to 1 and a non-zero mantissa, whereas positive and negative infinity have exponent bits set to 1 and a zero mantissa. Leveraging this property, we can efficiently detect whether any value has an exponent field of all 1s using bit-wise operations. If this condition is met, the value is considered to have overflowed; otherwise, it has not. This eliminates the need for intermediate values. Furthermore, as this operation is dependency-free, it can be parallelized to maximize performance. This fused overflow check achieves an

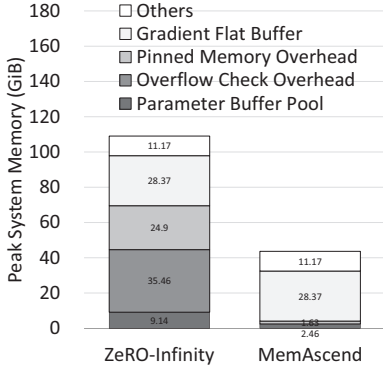


Fig. 6. Peak system memory usage comparison for training Qwen2.5-7B between ZeRO-Infinity and MemAscend.

average efficiency of approximately 97% across model sizes ranging from 1 billion to 32 billion parameters, and resolves the bottleneck issue that arises during overflow checks at large scale.

E. Direct NVMe Engine

The primary goal of the Direct NVMe Engine is to bypass the Linux filesystem overhead by using raw I/O to directly send asynchronous I/O (AIO) requests to the device driver via `iouring` or `libaio`. The overview of architecture and its workflow is shown in Figure 5.

First, the SSD offloading system issues a tensor AIO request. The request context contains a unique tensor name (as a key), a data pointer, and an offset aligned to the tensor size. Next, the Direct NVMe Engine distributes this request among multiple thread workers, dividing the data into equal portions for balanced performance. Each thread consults the Tensor Location Dictionary to determine which SSD device and logical block address (LBA) to use.

If the Tensor Location Dictionary has not recorded the tensor yet, it consults the Location Allocator for SSD space. This step ensures that data are horizontally partitioned across SSDs, effectively implementing striping in place of Software RAID 0. The Shared Device Information structure, implemented via shared memory, guarantees that multiple processes do not allocate overlapping SSD regions.

After each thread obtains its data pointer, offset, LBA, and raw SSD device path, it sends a raw AIO request through `libaio`. By applying load balancing, striping, and multi-threading, the Direct NVMe Engine reduces latency and achieves higher throughput compared to approaches that rely on filesystem-based AIO.

V. MEMORY EFFICIENCY AND PERFORMANCE ANALYSIS

MemAscend significantly reduces system memory usage compared to prior SSD offloading systems without sacrificing performance. Lower system memory consumption is key to reducing the cost of training tasks. Conserving system memory offers several key advantages. First, with equivalent hardware, this approach enables training models with more trainable parameters, thus achieving the same training setup at a lower

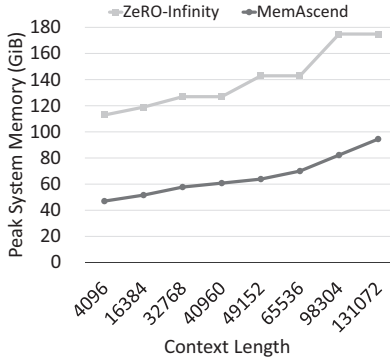


Fig. 7. Peak system memory usage comparison between ZeRO-Infinity and MemAscend across different context lengths.

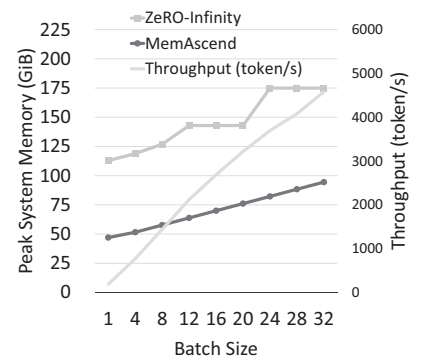


Fig. 8. Peak system memory usage and throughput comparison between ZeRO-Infinity and MemAscend across different batch sizes.

cost. Second, this method supports longer context lengths. Extended context lengths necessitate larger activation checkpointing values. By offloading this component from GPU memory to system memory, the available system memory enables these longer context lengths. Finally, this approach improves training performance. While a primary drawback of SSD offloading is the reduced training throughput stemming from PCIe transfer overhead, offloading also enables larger batch sizes. This boosts GPU efficiency by processing more data per batch. The following sections analyze memory efficiency in detail. Figure 6 shows the memory breakdown across system components during training of the Qwen2.5-7B model [30]. MemAscend shows notable improvements in the key areas of memory usage. The discussion then turns to how reduced memory requirements enable longer context lengths and larger batch sizes, both of which can contribute to higher throughput.

A. Memory Efficiency

MemAscend first introduces an Adaptive Buffer Pool to reduce memory fragmentation. For the Qwen2.5-7B model in fp16, this approach requires about 2.46GiB of memory for buffer allocations. In contrast, the standard SSD offloading method reserves a fixed 9.14GiB. This change cuts memory use in the parameter buffer pool by 73%. To eliminate peak memory spikes from overflow checking, MemAscend implements a Fused Overflow Check kernel. Conventional checks rely on intermediate buffers, adding a $1.25\times$ overhead and consuming 35.46GiB. The fused kernel maintains numerical stability without this overhead, reducing usage to 0GiB. SSD offloading also depends on pinned memory to move data between CPU and GPU. Traditional allocation uses power-of-two alignment, introducing significant waste. MemAscend applies a zero-overhead strategy that allocates only the required memory. This reduces pinned memory overhead from 24.90GiB to 1.63GiB, a 93.5% decrease. Some components remain constant across methods, including the Gradient Flat Buffer and small system allocations like optimizer state buffers and the swap-out buffer. These account for stable memory usage of roughly 28.37GiB and 11.17GiB, respectively. MemAscend brings total peak system memory usage down from 109.04GiB under ZeRO-Infinity to 43.64GiB, a 60% reduction. This

allows for training larger models and handling longer input sequences within the same memory budget.

B. Enable Larger Context Length

In the SSD offloading scenario, the key constraint in expanding the context length or batch size is the activation checkpoint value, which scales linearly with both parameters. To alleviate this GPU memory bottleneck, a pinned memory buffer on the CPU can be utilized to swap activation checkpoint values from GPU memory to system memory, potentially enabling longer context lengths. However, this shifts the bottleneck from GPU memory to system memory.

The total size of activation checkpointed values in system memory is calculated using the following formula, where we define N_g as the number of GPUs, B as the batch size, C as the context length, L as the number of layers, H as the hidden size, F_{16} as the bytes per fp16, and P_m as the pinned memory overhead. Here, the number of layers L accounts for the activation checkpointing enabled in each transformer layer.

$$N_g \times B \times C \times L \times H \times F_{16} + P_m \quad (1)$$

Figure 7 shows that the usage of system memory increases with increasing context length when running Qwen2.5-7B on two GPUs. Our MemAscend method scales linearly with context length, exhibiting minimal pinned memory overhead, meaning the increase is almost entirely due to context length scaling. In contrast, the original SSD offloading system scales more rapidly and begins with higher memory usage. This disparity arises because its pinned overhead aligns to the nearest power-of-two value, resulting in faster scaling and instances where different context lengths yield identical memory usage due to this alignment. Consequently, our method significantly reduces system memory consumption and slows the scaling rate with increasing context length, offering greater flexibility to extend context length without exhausting system memory. For example, with a 128 GiB system memory limit, the original SSD offloading system supports a context length of 16,384, while MemAscend scales up to 131,072 under the same configuration.

C. Enable Higher Performance

Our MemAscend not only supports a larger trainable context length, but also unlocks the potential for peak performance by enabling a larger batch size. A larger batch size allows the GPU to process more data within the same data transfer volume. In an SSD offloading scenario, performance degradation is primarily due to additional data transfers. By optimizing the ratio of tensor data computation to data transfer processing more data under the same transfer load, we can mitigate the drawbacks of SSD offloading. Specifically, a larger batch size means offloading and retrieving the same volume of data while computing more data, thus enhancing performance potential. As noted in the previous section, the size of the activation checkpoint values in the system memory follows Equation 1. Thus, with greater system memory availability, we can offload larger activation checkpointed values from the GPU, enhancing batch size potential.

TABLE II
HARDWARE SPECIFICATIONS FOR TWO CONFIGURATIONS

Component	Configuration 1	Configuration 2
CPU	Intel(R) Xeon(R) 6780E	2 x AMD EPYC 7282
CPU Memory	1TB 6400 MT/s DDR5	1TB 3200 MT/s DDR4
PCIe	Gen5	Gen4
GPU	2 x NVIDIA H100 PCIe w/o NVL	1 x NVIDIA A5000
SSD	1 x DapuStor Haishen5 H5100 7.5 TB	2 x Phison AI100E 2TB

In Figure 8, we compare the original SSD offloading system with our MemAscend method during Qwen2.5-7B training on two GPUs. Initially, we observe memory usage and scaling rates consistent with the previous section, as increasing batch size or context length equally impacts the size of activation checkpointed values. And our method exhibits significantly lower system memory requirements and a slower scaling rate across batch sizes. This reduced demand provides MemAscend with the flexibility to increase batch size without risking system memory exhaustion.

Next, we observe that throughput increases nearly linearly with batch size. This confirms that a larger batch size boosts overall performance, as we offload the same data volume while processing more computations. In summary, MemAscend improves performance potential by enabling larger batch sizes with increased data offloading to system memory. For instance, with a 128 GiB system memory limit, the original SSD offloading system supports a batch size of 4, while MemAscend achieves 32 or greater in the same configuration, delivering substantially greater performance.

VI. EXPERIMENTAL EVALUATION

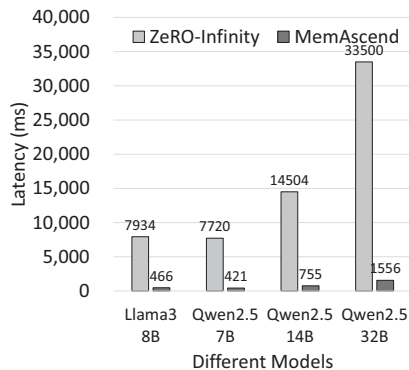
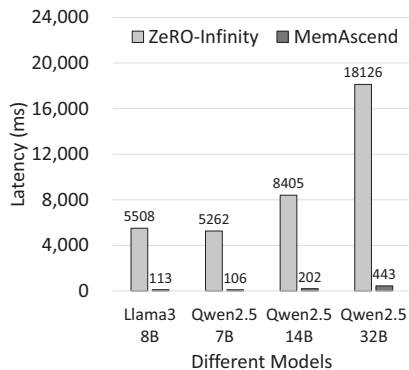
A. Setup

All experiments were carried out on two servers. Detailed hardware specifications are provided in Table II. MemAscend is evaluated using mixed-precision training of large language models with SSD offloading. The workloads vary by model architecture, context length, and batch size. Models include Llama3.1-8B and Qwen2.5, with parameter sizes of 7 billion, 14 billion and 32 billion. All models use the Hugging Face Transformers library (v4.46.3). The context lengths range from 4,096 to 131,072 tokens. Batch sizes vary across different experiments. The main evaluation metric is peak system memory usage during training. To assess overall performance, we also measure training throughput in tokens per second.

To evaluate the effectiveness of MemAscend, we compare it with ZeRO-Infinity. Both systems share a common setup to ensure fairness. Static memory components, including model parameters and optimizer states, are stored entirely on the SSD. To reduce GPU memory usage, we enable gradient checkpointing, Flash-Attention, and the Liger kernel. For experiments that require offloading gradient checkpoint activations, we use a modified version of Unsloth, adapted from its original single-GPU design.

B. Experimental Results

1) Assessment of Individual Methods:



(a) Configuration 1 with an Intel(R) Xeon(R) 6780E CPU (b) Configuration 2 with dual AMD EPYC 7282 CPUs

Fig. 9. Comparison of overflow check latency between ZeRO-Infinity and MemAscend across different CPU types and various models.

a) *Adaptive Buffer Pool*: As each model varies in weight tensor size due to differences in vocabulary size, hidden size, and other factors, this experimental section presents the memory usage of the Parameter Buffer Pool system across various models. The aim is to illustrate how the Adaptive Buffer Pool effectively reduces memory usage in different situations. The comparison is shown in Figure 11.

In these configurations, the Adaptive Buffer Pool consistently reduces memory usage by adjusting to the specific tensor sizes of each model, achieving an average reduction of 72.71% in different models. An interesting finding is that, for the Qwen2.5-14B and Qwen2.5-32B models, the original SSD offloading system uses the same amount of memory, while the Adaptive Buffer Pool shows slightly higher memory usage for the Qwen2.5-32B model. This occurs because the largest layer, the embedding layer, is identical in both the Qwen2.5-14B and Qwen2.5-32B models, leading to equal memory usage in the original system, which is limited by the largest layer size. However, in the Qwen2.5-32B model, the feedforward-related weights are larger, resulting in slightly increased memory usage compared to the Qwen2.5-14B. This finding highlights that the Adaptive Buffer Pool effectively reveals the actual memory needs of different models.

b) *Fused Overflow Check Kernel*: To assess the impact of the method described in Section IV-D, the analysis focuses on latency as a performance metric and memory efficiency compared to the implementation of the original SSD system. Figure 9(a) shows the overflow check latency across various models on Server Configuration 1, which uses an Intel(R) Xeon(R) 6780E CPU. In contrast, Figure 9(b) shows the corresponding results for Server Configuration 2, equipped with dual AMD EPYC 7282 CPUs. The latency scales linearly with model size, as the operation examines each gradient for overflow. The Fused Overflow Check Kernel, by removing intermediate tensor creation and multi-step processes, performs a single pass through the values, resulting in an average latency reduction of 97%. This kernel runs in every iteration that requires an update, with computational complexity scaling linearly with model size, underscoring the importance of performance optimization. For memory efficiency, Figure 10 indicates that MemAscend does not have additional memory

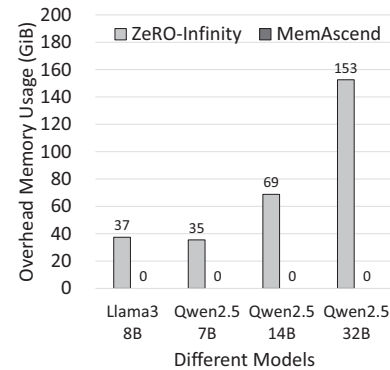


Fig. 10. Comparison of memory overhead for overflow checks between ZeRO-Infinity and MemAscend across different CPU types and various models.

overhead compared to ZeRO-Infinity. Unlike the original overflow check, which generates multiple intermediate values and incurs significant memory overhead, the fused kernel eliminates this overhead by avoiding intermediate computations entirely.

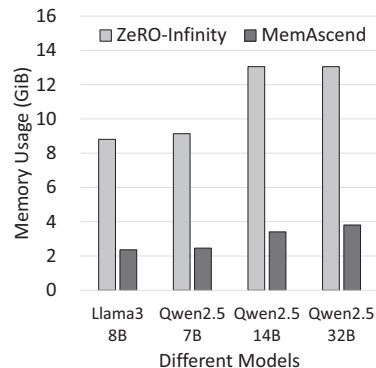


Fig. 11. Parameter buffer pool system memory usage comparison between ZeRO-Infinity and MemAscend across different LLM models.

c) *Direct NVMe Engine*: This evaluation examines the performance of the Direct NVMe Engine, described in Section IV-E, for SSD I/O in training scenarios with SSD offloading. The engine manages offloading of fp16 and fp32 model weights, gradients, and optimizer states. To determine suitable tensor sizes for benchmarking, model weight distributions were analyzed, excluding tensors too small to benefit from offloading. For instance, tensors with fewer than two million elements perform better in CPU memory. Common dense LLM architectures include several layers suitable for SSD offloading, such as feedforward layers, q, k, v, and o projection layers, the embedding layer, and the linear head layer. To ensure a precise comparison with the original SSD offloading system, tensor size ranges for fp16 and fp32 data were collected across various models. The analysis also considers multi-GPU setups, where data splits across processes. For example, a 100-million-element tensor divides into 50 million elements per process in a two-GPU configuration. Benchmarks used Configuration 2, as specified in Table II. The original SSD offloading system, reliant on filesystem I/O, utilized two SSDs in a RAID0 array formatted with ext4. By contrast, MemAscend employs the Direct NVMe Engine, which bypasses software RAID and sends requests directly to

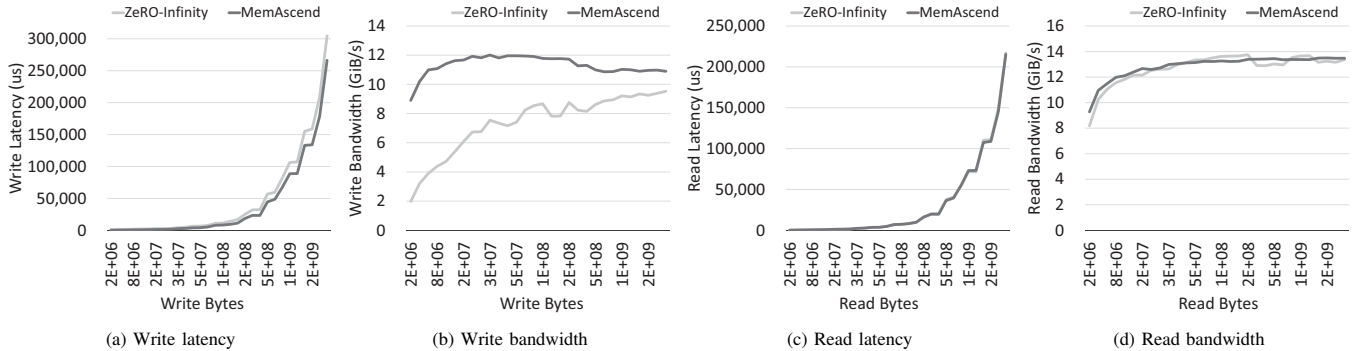


Fig. 12. Comparison of read and write latency and bandwidth between ZeRO-Infinity and MemAscend across various tensor sizes.

SSDs through the NVMe driver.

Figures 12(a) and 12(b) display write latency and bandwidth across tensor sizes. The Direct NVMe Engine consistently lowers write latency. For a 2,097,152-byte tensor, latency decreases from 988.222 microseconds to 219.418 microseconds, and for a 3,114,270,720-byte tensor, it drops from 304,604.779 to 266,212.637 microseconds. This improvement results from eliminating filesystem and RAID layer overhead. The engine also achieves higher write bandwidth across all tested sizes. As tensor sizes increase, the performance gap narrows, likely because filesystem and RAID overhead becomes less significant when host computation limits performance. Figures 12(c) and 12(d) show read latency and bandwidth. Read latency remains similar to the filesystem approach, as reads involve less overhead without costly allocation. However, the Direct NVMe Engine provides more consistent read bandwidth, while the filesystem-based method exhibits greater variability. The Direct NVMe Engine delivers superior write performance and more stable read throughput, surpassing the original SSD offloading system in SSD offloading training workflows.

2) Assessment of the Integrated Solution:

a) End-to-End Memory Efficiency: To evaluate the overall memory efficiency of our proposed MemAscend method, we present a comparison of peak system memory usage against the baseline ZeRO-Infinity system across four model architectures. This comparison is illustrated in Figure 13, a bar graph designed to highlight the system memory reduction achieved by our approach when activation checkpoint offloading is disabled. The x-axis of the figure represents the four model types, with each model featuring two bars: one for the baseline ZeRO-Infinity method and one for our MemAscend method. The y-axis denotes system memory usage, measured in GiB, providing a clear visual representation of memory consumption for each configuration.

The evaluation results reveal a consistent trend. MemAscend significantly reduces system memory usage across all models tested compared to the baseline. Specifically, for the Llama3.1-8B model, the baseline consumes 91.06 GiB, while our method reduces this to 44.71 GiB, a savings of approximately 50.9%. For the Qwen2.5-7B model, memory usage drops from 109.06 GiB to 43.67 GiB, leading to a reduction of 60.0%. In the Qwen2.5-14B case, the baseline requires 174.5 GiB, whereas MemAscend uses only 76.1 GiB, achieving a 56.4% decrease. Finally, for the Qwen2.5-32B

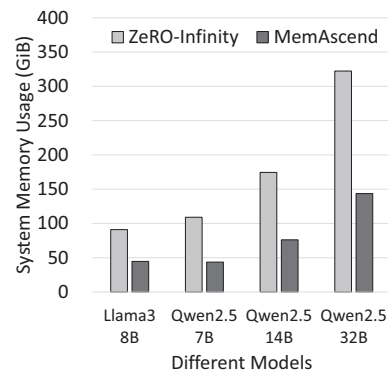


Fig. 13. Peak system memory usage comparison between ZeRO-Infinity and MemAscend across various models.

model, the baseline demands 322.3 GiB, while our method lowers this to 143.6 GiB, resulting in a reduction of 55.4%. On average, MemAscend achieves a memory reduction of approximately 55.7% across these models. This substantial memory savings underscores the effectiveness of our approach in optimizing resource utilization, with free memory allowing for further enhancements, such as supporting a longer context by utilizing the released space for activation checkpoint values, as discussed in the following sections. The effectiveness of MemAscend is the result of a combination of optimizations detailed in Section V-A.

b) Enabling Longer Context: Figure 14 illustrates the peak system memory usage in various context lengths for four models. Under a 2-GPU setup, we compare our MemAscend method with the baseline ZeRO-Infinity system across various models. In each figure, the x-axis represents the context length, ranging from 4,096 to 131,072 tokens, while the y-axis denotes system memory usage in GiB. These figures aim to demonstrate how our method reduces memory consumption, enabling support for longer context lengths under the same hardware configuration.

The general trend across all figures reveals that system memory usage increases with context length for both the baseline and our method. However, MemAscend consistently exhibits lower memory usage and a slower scaling rate compared to ZeRO-Infinity. For example, in Figure 14(a) for Llama3.1-8B, the baseline memory usage increases from 94.88 GiB at 4,096 tokens to 156.88 GiB at 131,072 tokens, while our method increases from 48.67 GiB to 110.67 GiB. Similarly, in Figure 14(d) for Qwen2.5-32B, the baseline

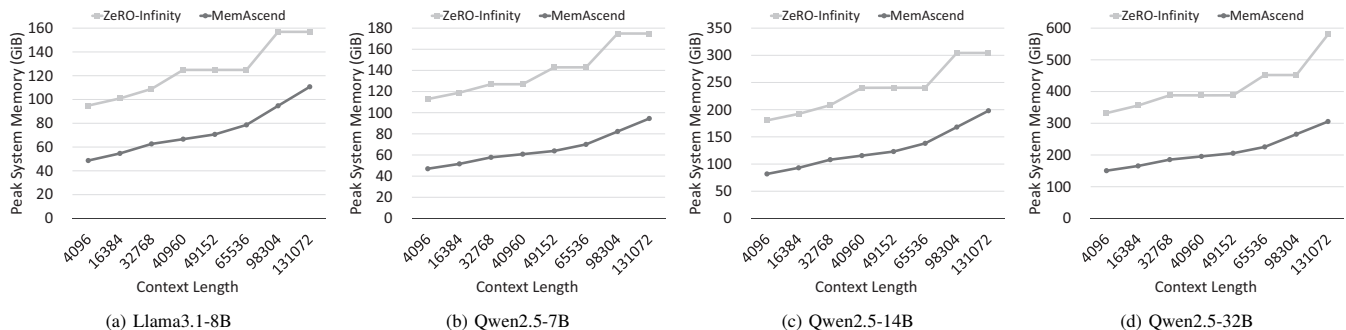


Fig. 14. Comparison of peak system memory usage between ZeRO-Infinity and MemAscend in a 2-GPU setup, with context lengths ranging from 4,096 to 131,072 tokens. The results demonstrate MemAscend ability to lower memory consumption significantly, allowing training with longer context lengths that ZeRO-Infinity cannot support within the same hardware constraints.

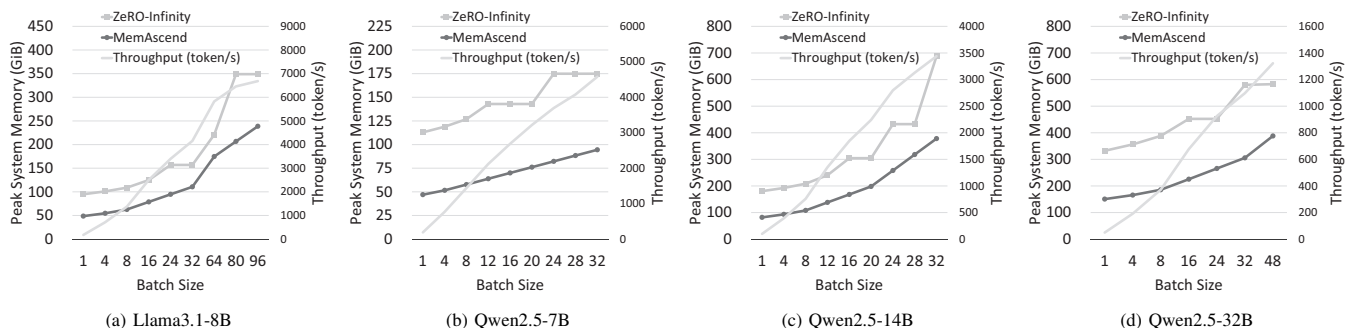


Fig. 15. System memory usage and throughput were compared between ZeRO-Infinity and MemAscend across varying batch sizes, using a fixed context length of 4,096 tokens on a 2-GPU setup with NVIDIA H100s. MemAscend maintained lower system memory usage across all batch sizes, enabling efficient scaling to larger batches. This allowed the system to reach saturated throughput without breaching memory constraints, while ZeRO-Infinity exhibited earlier memory bottlenecks that limited batch size and overall performance.

jumps from 332.12 GiB to 580.12 GiB, while MemAscend scales from 150.51 GiB to 305.5 GiB. The effectiveness of MemAscend is the result of a combination of optimizations detailed in Section V-B.

c) Enabling Higher Performance by Utilizing Memory Space: To evaluate how our MemAscend method enhances performance by leveraging memory savings, we present Figure 15, which comprises four subfigures illustrating memory usage and throughput across different batch sizes for four models. Each subfigure corresponds to one model, with the x-axis representing batch size (ranging from 1 to 96, depending on the model), the left y-axis indicating system memory usage in GiB, and the right y-axis showing throughput in tokens per second (tokens/s). In each subfigure, three lines are plotted: one for throughput trends, one for baseline system memory usage, and one for our method system memory usage. These results were obtained using Configuration 1 (2 NVIDIA H100 GPUs) with a fixed context length of 4,096 tokens.

The general trend observed in all the subfigures is two-fold. First, system memory usage increases with batch size for both the baseline and MemAscend, reflecting the growing demand for activation checkpointed values as batch size scales (see Equation 1). However, MemAscend consistently consumes significantly less memory than the baseline across all models and batch sizes. For example, in the Llama3.1-8B subfigure, the baseline memory usage rises from 94.89 GiB at batch size 1 to 348.91 GiB at batch size 96, while MemAscend increases from 48.67 GiB to 238.69 GiB. Similar patterns

are evident in the Qwen2.5 models, with memory savings becoming more pronounced at larger batch sizes. Across all models, MemAscend achieves an average memory reduction of approximately 42.8%, enabling support for larger batch sizes under the same system memory constraints. Second, throughput increases near-linearly with batch size for all models, demonstrating that larger batch sizes enhance GPU utilization. For example, in the Qwen2.5-32B subfigure, the throughput grows from 49.32 tokens/s at batch size 1 to 1,322.55 tokens/s at batch size 48, highlighting the performance potential unlocked by larger batch sizes. This shows that our training system can achieve higher throughput under identical configurations by better utilizing GPU resources through larger batch sizes. The effectiveness of MemAscend is due to its ability to optimize system memory usage, as detailed in Section V-C.

d) End-to-End Performance Improvement: We evaluated the end-to-end performance of MemAscend by comparing its training throughput against the ZeRO-Infinity baseline under two hardware configurations described in Table II. Both systems were tested with Direct NVMe Engine enabled. ZeRO-Infinity without this engine, which relies on a traditional filesystem-based approach, is unstable and prone to hanging, so it was excluded from this comparison. Table III reports the percentages of improvement in performance in a range of models, batch sizes, and hardware configurations, along with the gains achieved by MemAscend over ZeRO-Infinity. All tests used a fixed context length of 4096. For each configuration, we

TABLE III
END-TO-END PERFORMANCE IMPROVEMENT FROM ZERO-INFINITY TO MEMASCEND FOR CONFIGURATIONS 1 (C1) AND 2 (C2)

Model Name	Batch (C1 / C2)	C1 Improvement (%)	C2 Improvement (%)
Llama3.1-8B	8 / 8	6.97	12.91
Llama3.1-8B	80 / 20	2.72	7.52
Qwen2.5-7B	8 / 8	5.53	14.02
Qwen2.5-7B	64 / 20	3.73	8.36
Qwen2.5-14B	8 / 4	6.45	18.86
Qwen2.5-14B	64 / 16	3.28	6.77
Qwen2.5-32B	8 / 4	5.64	18.43
Qwen2.5-32B	48 / 8	2.89	16.42

include several batch sizes to capture workload variation. The table lists the model, the batch sizes used for Configurations 1 and 2, and the corresponding percentage improvements.

In both configurations, MemAscend consistently outperformed ZeRO-Infinity, with improvements ranging from 2.72% to 6.97% in Configuration 1. In Configuration 2, the gains were more substantial, ranging from 6.77% to 18.86%. This difference underscores a key observation: MemAscend advantages are more pronounced when the baseline suffers from higher latency in overflow checking, as in Configuration 2, where slower CPU performance increases the cost of overflow checking. Notably, performance gains tend to be larger at smaller batch sizes. For example, Qwen2.5-14B shows an improvement of 18.86% at batch size 4 in Configuration 2 and 6.77% at batch size 16. This trend suggests that when batch sizes are smaller and forward and backward pass times are reduced, the relative impact of our optimizations becomes more significant.

3) *Extended Experiments*: This section presents additional experiments that fall outside the main scope of the paper. The first explores the use of bf16 precision for optimizer-related values. This setup differs from the baseline, which relies on fp32 for those values as part of fp16 mixed-precision training with SSD offloading. Because of this difference in numerical precision, the results are not directly comparable to those of ZeRO-Infinity. Nonetheless, enabling bf16 for optimizer states shows promising improvements, especially in reducing I/O load in SSD offloading systems. The second subsection examines mixed-precision training with bf16 instead of the fp16-based setup used in the main experiments. This test demonstrates the method’s adaptability and effectiveness in a bf16 training environment. Together, these experiments highlight MemAscend’s flexibility and stability across different precision.

a) *bf16 Half-Precision Optimizer*: The original baseline supported only fp32 optimizer states. Recent work has investigated lower-precision alternatives, including 8-bit [15] and 4-bit [16] formats. These reduced-precision representations are especially useful in SSD offloading systems, where lowering the I/O demand is critical. To explore this benefit, we further added bf16 optimizer support to MemAscend. We evaluate its impact by comparing I/O volume per iteration (Figure 16) and end-to-end throughput improvements (Table IV) between Configurations 1 and 2, using a fixed context length of 4096 across four models. The evaluation results show that integrating bf16 into MemAscend consistently improves throughput across all tested models and configurations. For Configuration 1, the average throughput gain is 27.25%, peaking at 56.80% for

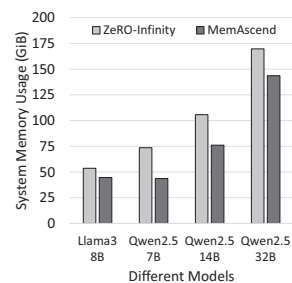
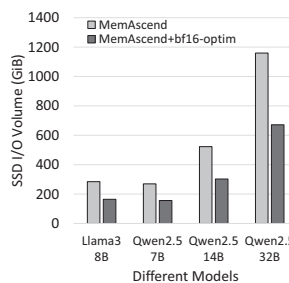


Fig. 16. Comparison of total I/O volume per iteration for MemAscend and MemAscend with bf16 optimizer. Fig. 17. Comparison of peak system memory usage for ZeRO-Infinity and MemAscend in bf16 mixed-precision training across various models.

TABLE IV
THROUGHPUT IMPROVEMENT FROM USING BF16 OPTIMIZER IN MEMASCEND FOR CONFIGURATIONS 1 (C1) AND 2 (C2)

Model Name	Batch (C1 / C2)	C1 Improvement (%)	C2 Improvement (%)
Llama3.1-8B	8 / 8	28.63	19.39
Llama3.1-8B	80 / 20	13.24	11.99
Qwen2.5-7B	8 / 8	56.80	18.26
Qwen2.5-7B	64 / 20	22.55	9.99
Qwen2.5-14B	8 / 4	28.84	22.11
Qwen2.5-14B	64 / 16	16.73	11.80
Qwen2.5-32B	8 / 4	33.26	24.21
Qwen2.5-32B	48 / 8	17.92	18.87

Qwen2.5-7B with a batch size of 8, and dipping to 13.24% for Llama3.1-8B with a batch size of 80. Configuration 2 shows an average improvement of 17.08%, ranging from 9.99% for Qwen2.5-7B at batch size 20 to 24.21% for Qwen2.5-32B at batch size 4. These performance gains stem from lower I/O overhead, as shown in Figure 16, where bf16 usage significantly reduces I/O volume per iteration. The improvements are more pronounced at smaller batch sizes, where I/O bottlenecks dominate. In contrast, larger batches increase computation time, masking I/O savings. These results underscore the effectiveness of bf16 in optimizing SSD offloading systems.

b) *bf16 Mixed-Precision Training*: This section focuses on mixed-precision training. Although fp16 mixed-precision training has been widely used, bf16 mixed-precision training for GPU computation has recently gained popularity as an alternative approach. Both methods have their advantages and disadvantages. fp16 offers higher precision and supports a wider range of GPUs but requires gradient overflow checks, whereas our method minimizes the overhead associated with this process. In contrast, bf16 provides lower precision and requires newer GPU architectures (post-Ampere), but offers greater stability. To demonstrate the memory efficiency of our MemAscend approach in mixed-precision training of bf16, refer to Figure 17. Our method achieves an average memory reduction of 25.19%. However, since bf16 does not need to mitigate peak overflow issues, the average memory reduction is lower than that of fp16 mixed-precision training, where the average reduction reaches 55.7%.

VII. CONCLUSION

MemAscend revisits SSD offloading fine-tuning from the perspective of system memory, revealing that system memory is often the true bottleneck on commodity machines. It identifies several hidden sources of overhead: buffer pool

fragmentation, over-aligned pinned allocations, overflow check memory spikes, and filesystem I/O overhead. To address these issues, MemAscend introduces an Adaptive Buffer Pool, Zero-overhead Allocation, a single-pass Fused Overflow Check kernel, and a Direct NVMe Engine. These optimizations reduce parameter buffer waste by up to 72.7% and decrease overall peak system memory usage by 55.7%. MemAscend also eliminates the 1.25× overflow check memory overhead and reduces its latency by 9%. With the saved memory, MemAscend enables training of larger models, longer context lengths, and higher batch sizes on the same hardware, making full-parameter LLM fine-tuning more accessible to smaller labs and independent practitioners.

REFERENCES

- [1] S. Minaee, T. Mikolov, N. Nikzad *et al.*, “Large language models: A survey,” *arXiv preprint arXiv:2402.06196*, 2025. [Online]. Available: <https://arxiv.org/abs/2402.06196>
- [2] S. Zhang, L. Dong, X. Li, S. Zhang, X. Sun, S. Wang, J. Li, R. Hu, T. Zhang, F. Wu, and G. Wang, “Instruction tuning for large language models: A survey,” *arXiv preprint arXiv:2308.10792*, 2024. [Online]. Available: <https://arxiv.org/abs/2308.10792>
- [3] A. Grattafiori, A. Dubey, A. Jauhri *et al.*, “The llama 3 herd of models,” *arXiv preprint arXiv:2407.21783*, 2024. [Online]. Available: <https://arxiv.org/abs/2407.21783>
- [4] S. Rajbhandari, J. Rasley, O. Ruwase, and Y. He, “Zero: Memory optimizations toward training trillion parameter models,” in *Proceedings of the International Conference for High Performance Computing, Networking, Storage and Analysis*, 2020.
- [5] D. P. Kingma and J. Ba, “Adam: A method for stochastic optimization,” *International Conference on Learning Representations*, 2014.
- [6] Y. Li, A. Phanishayee, D. Murray, J. Tarnawski, and N. S. Kim, “Harmony: overcoming the hurdles of gpu memory capacity to train massive dnn models on commodity servers,” *Proceedings of the VLDB Endowment*, 2022. [Online]. Available: <http://dx.doi.org/10.14778/3551793.3551828>
- [7] T. Chen, B. Xu, C. Zhang, and C. Guestrin, “Training deep nets with sublinear memory cost,” *arXiv preprint arXiv:1604.06174*, 2016. [Online]. Available: <https://arxiv.org/abs/1604.06174>
- [8] P.-L. Hsu, Y. Dai, V. Kothapalli *et al.*, “Liger kernel: Efficient triton kernels for llm training,” *arXiv preprint arXiv:2410.10989*, 2025. [Online]. Available: <https://arxiv.org/abs/2410.10989>
- [9] B. Zhang and R. Sennrich, “Root mean square layer normalization,” *Advances in Neural Information Processing Systems*, vol. 32, 2019.
- [10] N. Shazeer, “Glu variants improve transformer,” *arXiv preprint arXiv:2002.05202*, 2020.
- [11] Z. Zhang and M. Sabuncu, “Generalized cross entropy loss for training deep neural networks with noisy labels,” *Advances in neural information processing systems*, vol. 31, 2018.
- [12] Welcome to triton’s documentation! — triton documentation. [Online]. Available: <https://triton-lang.org/main/index.html>
- [13] P. Micikevicius, S. Narang, J. Alben, G. Diamos, E. Elsen, D. Garcia, B. Ginsburg, M. Houston, O. Kuchaiev, G. Venkatesh, and H. Wu, “Mixed precision training,” *arXiv preprint arXiv:1710.03740*, 2018. [Online]. Available: <https://arxiv.org/abs/1710.03740>
- [14] T. Dao, D. Fu, S. Ermon, A. Rudra, and C. Ré, “Flashattention: Fast and memory-efficient exact attention with io-awareness,” *Advances in neural information processing systems*, 2022.
- [15] T. Dettmers, M. Lewis, S. Shleifer, and L. Zettlemoyer, “8-bit optimizers via block-wise quantization,” *arXiv preprint arXiv:2110.02861*, 2022. [Online]. Available: <https://arxiv.org/abs/2110.02861>
- [16] B. Li, J. Chen, and J. Zhu, “Memory efficient optimizers with 4-bit states,” in *Thirty-seventh Conference on Neural Information Processing Systems*, 2023. [Online]. Available: <https://openreview.net/forum?id=nN8TnHB5nw>
- [17] Z. Han, C. Gao, J. Liu, J. Zhang, and S. Q. Zhang, “Parameter-efficient fine-tuning for large models: A comprehensive survey,” *Transactions on Machine Learning Research*, 2024. [Online]. Available: <https://openreview.net/forum?id=IIsCS8b6zj>
- [18] E. J. Hu, Y. Shen, P. Wallis, Z. Allen-Zhu, Y. Li, S. Wang, L. Wang, and W. Chen, “LoRA: Low-rank adaptation of large language models,” in *International Conference on Learning Representations*, 2022. [Online]. Available: <https://openreview.net/forum?id=nZeVKeeFYf9>
- [19] D. Biderman, J. Portes, J. J. G. Ortiz, M. Paul, P. Greengard, C. Jennings, D. King, S. Havens, V. Chiley, J. Frankle, C. Blakeney, and J. P. Cunningham, “Lora learns less and forgets less,” *Transactions on Machine Learning Research*, 2024. [Online]. Available: <https://openreview.net/forum?id=aloEru2qCG>
- [20] R. Shuttleworth, J. Andreas, A. Torralba, and P. Sharma, “Lora vs full fine-tuning: An illusion of equivalence,” *arXiv preprint arXiv:2410.21228*, 2024. [Online]. Available: <https://arxiv.org/abs/2410.21228>
- [21] S. Rajbhandari, O. Ruwase, J. Rasley *et al.*, “Zero-infinity: Breaking the gpu memory wall for extreme scale deep learning,” in *Proceedings of the international conference for high performance computing, networking, storage and analysis*, 2021.
- [22] C. Liao, M. Sun, Z. Yang, J. Xie, K. Chen, B. Yuan, F. Wu, and Z. Wang, “Lohan: Low-cost high-performance framework to fine-tune 100b model on a consumer gpu,” *arXiv preprint arXiv:2403.06504*, 2024. [Online]. Available: <https://arxiv.org/abs/2403.06504>
- [23] H. Jang, J. Song, J. Jung, J. Park, Y. Kim, and J. Lee, “Smart-infinity: Fast large language model training using near-storage processing on a real system,” in *2024 IEEE International Symposium on High-Performance Computer Architecture (HPCA)*, 2024.
- [24] M. Harris. (2012) How to optimize data transfers in cuda c/c++. [Online]. Available: <https://developer.nvidia.com/blog/how-optimize-data-transfers-cuda-cc/>
- [25] Microsoft. Deepspeed. [Online]. Available: <https://www.deepspeed.ai/>
- [26] J. Ren, S. Rajbhandari, R. Y. Aminabadi *et al.*, “Zero-offload: Democratizing billion-scale model training,” in *2021 USENIX Annual Technical Conference (USENIX ATC 21)*, 2021.
- [27] K. Wu, J. B. Park, X. Zhang *et al.*, “Ssdtrain: Faster large language model training using ssd-based activation offloading,” in *Design Automation Conference (DAC)*, 2025.
- [28] Unsloth. (2025) Unsloth gradient checkpointing - 4x longer context windows. [Online]. Available: <https://unsloth.ai/blog/long-context>
- [29] IEEE, “Ieee standard for floating-point arithmetic,” *IEEE Std 754-2008*, pp. 1–70, 2008.
- [30] Qwen, :, A. Yang, B. Yang *et al.*, “Qwen2.5 technical report,” *arXiv preprint arXiv:2412.15115*, 2025. [Online]. Available: <https://arxiv.org/abs/2412.15115>